Available online at www.sciencedirect.com
SCIENCE DIRECT®
Quaternary Research 62 (2004) 60–75
QUATERNARY RESEARCH
www.elsevier.com/locate/yqres

Geochemical characterization, correlation, and optical dating of tephra in alluvial sequences of central western Argentina

Phillip S. Toms,[a,*,1] Matthew King,[a] Marcelo A. Zárate,[b] Rob A. Kemp,[a] and Franklin F. Foit Jr.[c]

[a] *Department of Geography, Royal Holloway, University of London, Surrey TW20 0EX, UK*
[b] *CONICET–Universidad Nacional de la Pampa, 6300 Santa Rosa, Argentina*
[c] *Geology Department, Washington State University, Pullman, WA 99164-6420, USA*

Received 7 March 2002

Abstract

The synthesis of paleoclimatic archives provided by loess and alluvial sequences of central Argentina has been hindered by the lack of a cohesive lithostratigraphic framework extending across the Chaco–Pampean plains and catchments of the Rios Desaguadero, Colorado, and Negro. This condition originates in part from the dearth of absolute chronological controls. The occurrence of discrete tephra layers across this region may provide an opportunity to address this deficiency if a tephrochronological framework can be established. The potential of such a project is assessed within the context of a pilot study constrained within alluvial sequences of central western Argentina proximal to potential source vents in the Southern Volcanic Zone. The intersite discrimination and correlation of tephra layers on a geochemical basis is examined, with indirect chronological control for the eruption of each generated by optical dating. Alluvial sediments on either side of each of five tephra units at a type site were dated using the optically stimulated luminescence of fine-silt-sized quartz, thus providing an age control on each tephra (ca. 24,000, 30,000, 32,000, 39,000, and 48,000 yr). The geochemical composition of each tephra was derived. Using these data, tephra layers at other sites in the study area were geochemically analyzed and, in instances of statistical concordance in major oxide structure, correlated to the type site and therefore ascribed ages. This methodology identified a further sixth volcanic event between ca. 24,000 and 30,000 yr not registered by type-site tephras. The extension of this initial tephrochronological framework beyond the alluvial sequences of central western Argentina is encouraged by the occurrence of geochemically distinct tephra verified and dated in this study.

Keywords: Mendoza; Argentina; Tephrochronology; Optical dating; Alluvial sequences

Introduction

Individual tephra layers can be used as chronostratigraphic marker horizons provided that their ages can be ascertained and the geochemical composition of their glasses is sufficiently distinct to allow differentiation and correlation between sites (Busacca et al., 1992; Davies et al., 2002; Foit et al., 1993; Gronvold et al., 1995; King et al., 2001; Turney et al., 2001). These isochronous deposits supply indirect chronological control for sites and can assist in elucidating the relative timing of regional environmental change (Davies et al., 2002; Turney et al., 2001).

Within Argentina, although widespread across Patagonia, the Pampas, and the Chaco region, tephras have not been the focus of detailed tephrochronological studies. Exceptions include the work of Auer (1974), which attempted to establish a preliminary Holocene tephrochronology in southernmost Patagonia and Tierra del Fuego. Stern (1990, 1992) subsequently contributed significantly to tephra studies in southern Argentina by providing information on the geochemistry, mineralogical composition, numerical ages, and source vents for a number of the Holocene tephra layers (Fig. 1). Other studies have focused on the middle Pleistocene eruptions of the Southern Volcanic Zone (Guerstein, 1993; Stern et al., 1984).

In central Argentina, tephras have been reported from a number of different localities across the Chaco–Pampean

* Corresponding author. Fax: +44-0-1242-543283.
E-mail address: ptoms@glos.ac.uk (P.S. Toms).
[1] Present address: Geochronology Laboratories, School of Environment, University of Gloucestershire, Swindon Road, Cheltenham, Gloucestershire GL50 4AZ, UK.

0033-5894/$ - see front matter © 2004 University of Washington. All rights reserved.
doi:10.1016/j.yqres.2004.05.005

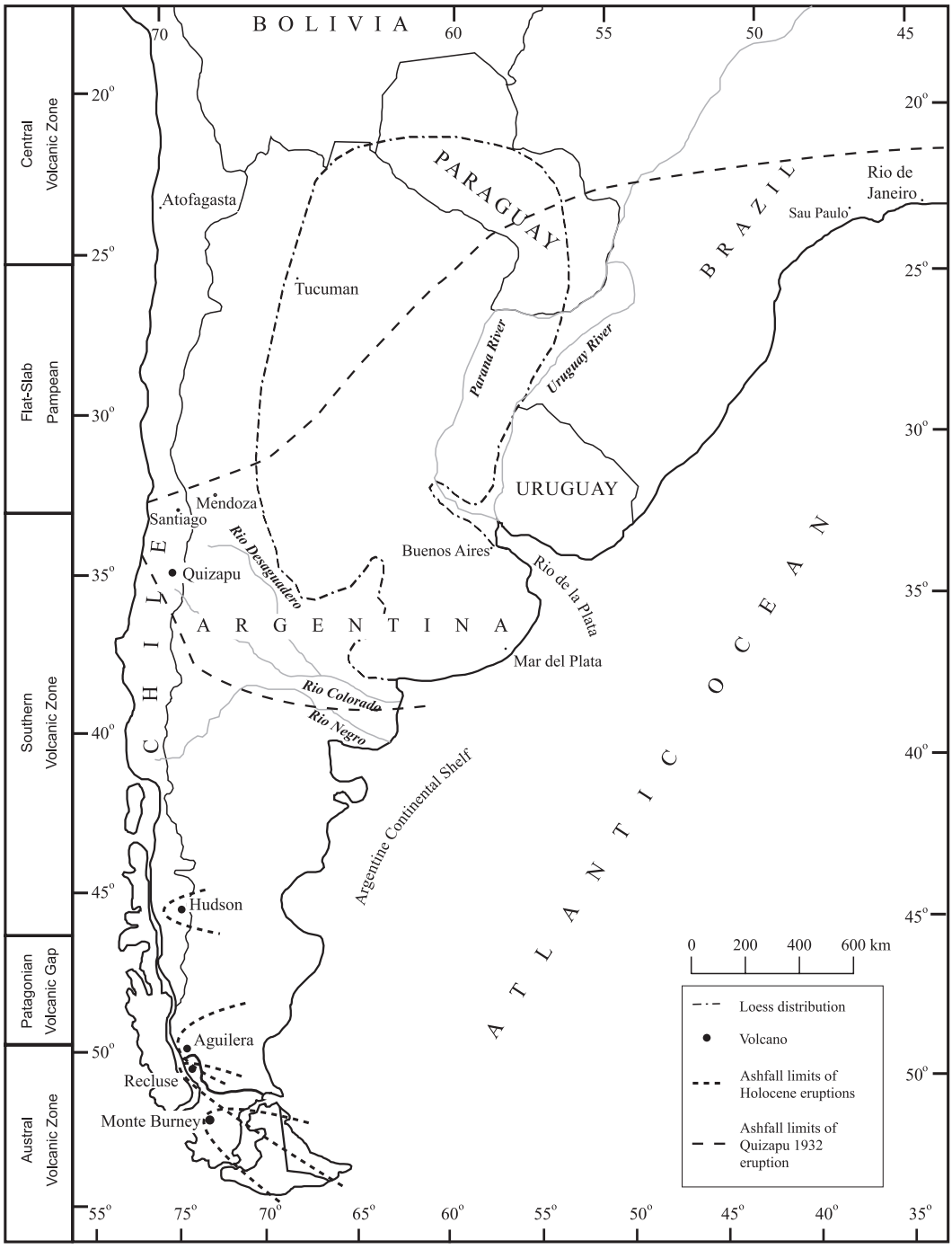

Fig. 1. Known fallout pattern for 1932 eruption of Quizapu and fallout models for ejecta from Holocene volcanic events relative to the distribution of loess and broad catchment areas of the Rios Desaguadero, Colorado, and Negro.

plain, either as discrete layers interstratified within loess (Imbellone and Camilión, 1988; Kraglievich, 1952; Morrás, 1994) and alluvial (Polanski, 1963) deposits or as high percentages of fresh volcanic material within individual loess units (Blasi et al., 2001; González Bonorino, 1965, Nabel et al., 1999). These windblown and waterlain deposits are important archives of Quaternary environmental change. The significance of Argentinian loess (Fig. 1) was identified by Terrugi (1957). Subsequent studies have reported the presence of one or more paleosols within these aeolian sequences (e.g., Kemp and Zárate, 2000; Kröhling, 1999; Teruggi and Imbellone, 1987; Zárate and Blasi, 1991; Zárate et al., 2002) extending in age as far back as the Pliocene (Kemp and Zárate, 2000). Given the contribution of similar loess–paleosol sequences in the Northern Hemisphere to knowledge of Quaternary climate change (e.g., Kukla, 1989), and in the context of establishing interhemispheric relationships during this period, the study of Argentinian

loess–paleosols is of critical importance. Alluvial sequences in the region also evidence past environmental change. For example, those to the south of Buenos Aires in the southern Pampas region contain an important record of both local and regional paleoenvironmental change during the late Quaternary (Bonadonna et al., 1995; Prieto, 1996, 2000; Quatrocchio and Borromei, 1998; Zárate et al., 2002).

However, assessment of past environmental change from these deposits is made problematic by the lack of a cohesive lithostratigraphic framework extending across the entire Chaco–Pampean plain, owing to a paucity of exposures of sufficient resolution and a limited number of absolute chronological controls (Muhs and Zárate, 2001). Given the presence of discrete layers of tephra in loess and alluvial deposits of central Argentina, the development of a tephrochronological framework may establish a chronostratigraphic foundation that assists the clarification of regional paleoenvironmental change.

The value of any tephrochronological framework in elucidating the relative timing of regional paleoenvironmental change is in part governed by the areal extent of ashfall, regulated by the location of the erupted source and wind velocity that prevailed during and shortly after the eruption. Active volcanoes in South America are limited to the Andean volcanic zones (Fig. 1). With respect to central Argentina, the dispersal pattern of ejecta from Andean eruptions would be influenced at present by southerly winds prevailing along the eastern margin of the Andes, modulated by westerlies across the southern Pampa in winter owing to the northward displacement of the subtropical high-pressure belt (Prohaska, 1976). The limits of ashfall reported for the 1932 eruption of Quizapu (Hildreth and Drake, 1992; Kittl, 1933; Larsson, 1937) illustrate this control (Fig. 1). Estimation of ejecta dispersal patterns relating to past eruptions requires an assessment of altered wind vectors associated with climate change. Suggestions of a significant northward shift of the Polar Front during glacials of the Quaternary period, generating westerlies of increased frequency and force across central Argentina (Heusser, 1991; Iriondo, 1993, 1999, 2000), are supported by the recent isotopic study of loess provenance by Smith et al. (2003). Hence, it is plausible to suggest that discrete tephra layers reported within loess sequences of the Chaco–Pampean plain and alluvial sediments of the Desaguadero, Colorado, and Negro catchments reflect fallout from volcanoes located directly west in the Southern Volcanic Zone (Fig. 1).

Here, the feasibility of establishing a tephrochronological framework for central Argentina is examined within the context of a pilot study sited in the area of Andean Piedmont west of Mendoza. This locality is proximal to volcanoes of the Southern Volcanic Zone known to have been active during the Late Pleistocene–Holocene and possesses a number of visible tephra horizons formed from primary fallout of temporally distinct volcanic events. The paleoenvironmental significance of deposits in this area and the present difficulties in ascribing a temporal framework are outlined. Addressing these deficiencies is attempted first through luminescence dating and geochemically characterising a series of tephra layers exposed within an alluvial sequence to form a type site, and then geochemically correlating them to undated layers at other sites in the area.

Palaeoclimatic significance of study area

Similar, yet thicker, alluvial sequences to those south of Buenos Aires, have recently been identified within the Andean Piedmont of Mendoza (33°S, 69°W; Fig. 1), 1500 km to the west of the southern Pampas (Zárate, 2000, 2002). The piedmont is situated in a region that is thought to have been climatically sensitive to the latitudinal shift of the Pacific and Atlantic anticyclonic centers during the Late Pleistocene and Holocene (Vázquez et al., 2000), though evidence is largely limited to a few pollen records from a rockshelter (D'Antoni, 1983) and Holocene peat deposits (Markgraf, 1983). It has further significance in that it is located within the provenance area of the eolian deposits covering the central part of Argentina (Clapperton, 1993; Iriondo, 1997; Smith et al., 2003; Teruggi, 1957). Despite the key location of the Andean Piedmont, however, there have been no detailed studies of the alluvial sequences within the region. Two of the major limitations have been the lack of chronological controls and a regional lithostratigraphic framework. Radiocarbon dating of paleosols at a number of sites has enabled the upper parts of the sequences to be assigned a Holocene age and be correlated with units in the southern Pampas (Zárate, 2002). The dearth of organic material in the underlying 10–20 m of sediments, however, precludes any extension of this radiocarbon chronology. Furthermore, attempts to establish a lithostratigraphic framework (Polanski, 1963) have been unsuccessful due to the comparatively uniform characteristics of these thick alluvial silty sands and lateral facies changes, altering the characteristics of individual units (Zárate, 2002).

Site descriptions and sampling

The sites studied are located in a longitudinal graben with 1500 to 1800 m of Miocene to Pleistocene sedimentary infilling that forms a low-relief plain descending from 1100 to 850 m above sea level. All the sites are cliff sections within steep-sided valley gorges of tributaries of the Rio Tunuyán, which drain the eastern Andean piedmont, and are located approximately 70 km south of the city of Mendoza (Figs. 1 and 2).

The study area is located in the piedmont of the northernmost segment of the Southern Volcanic Zone, which extends from 33°30′S to 46° 30′S (Ramos and Almeida, 2000). This volcanic district is characterized by dacitic to

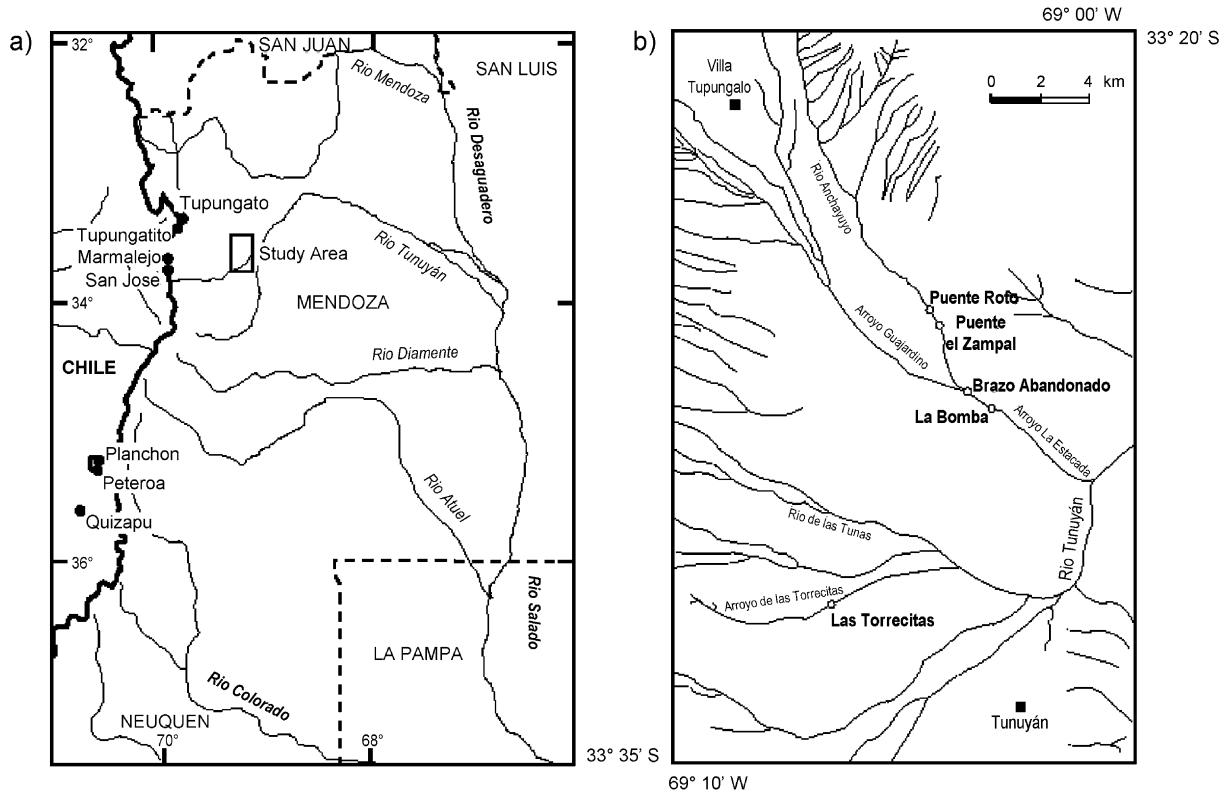

Fig. 2. (a) Location of study area relative to potential source volcanoes of the Southern Volcanic Zone active during the Late Pleistocene–Holocene. (b) Study area and site location map.

andesitic stratovolcanoes between 33° to 37°S (Fig. 2a; Ramos and Nullo, 1993). The Quaternary volcanism begins with the Pleistocene eruption of the Tupungato volcano (33°15′S), while recent and active volcanism is limited to the volcanoes Marmolejo, San José, and Tupungatito, 70 to 80 km west of the studied area (Fig. 2a). Another active volcanic area, encompassing the Calabozos caldera complex and the Azufre–Planchon–Peteroa volcanic center, is situated 200–300 km further south. It has an important record of mid-Pleistocene to historical eruptions (Hildreth et al., 1984; Naranjo et al., 1999) as recent as those of Quizapu in 1932 (Hildreth and Drake, 1992) and Peteroa in 1991 (Fig. 2a). East of the Andean volcanic chain, an extensive back arc basaltic field is developed between 35° and 37°S covering southern Mendoza and neighboring provinces, with records of Pliocene to Holocene volcanic activity represented by lava fields and monogenetic cinder cones (Inbar and Risso, 2001). The volcanoes listed here are postulated as potential sources of tephras outlined in this inquiry on the basis of position relative to the study area and in consideration of wind vectors likely prevailing during the period of active volcanism. No attempt has been made to identify the source vents directly.

The type site of Las Torrecitas (Fig. 2b), developed in this study, comprises an 18 m vertical section (Fig. 3) consisting of massive (units 2, 4, 6, and 8) and weakly cross-bedded (units 3, 5, and 7) fluvial silty sands capped by a thin fine sandy eolian mantle (unit 1). Five discrete interbedded tephra layers (TOR-1 to 5, Fig. 3), with sharp basal boundaries, can be readily observed in the field and traced along the valley side up- and downstream for more than 1 km. Each of the tephra were sampled in March 2001 for electron microprobe (EMP) analysis with undisturbed blocks for optical dating taken approximately 30 cm to either side of each layer (Fig. 3).

Additional sites where tephra layers have been sampled for EMP analysis are within 10 to 13 km of Las Torrecitas along the valley sides of the Anchayuyo–La Estacada system (Fig. 2b). In all cases, tephra layers can be traced for several kilometers along adjacent sections both up- and downstream, thus removing the possibility that they have been fluvially reworked and do not represent their original air-fall stratigraphic positions. Three distinct tephra layers were sampled at Brazo Abandonado (Fig. 2b), the lowermost being differentiated into three subunits on the basis of color (Fig. 4). A similar thick color-layered tephra occurred at the base of the section of Puente el Zampal (Figs. 2b and 4). In both cases, bulk and (wherever feasible) subunit samples were taken of these basal tephra to ascertain whether the color variations reflect primary tephra characteristics or postdepositional redistribution of redox elements (e.g., Fe, Mn). Bulk and lower/upper samples were also taken from the tephra at La Bomba (Figs. 2b and 4), though this time the purpose of the subsamples was to determine

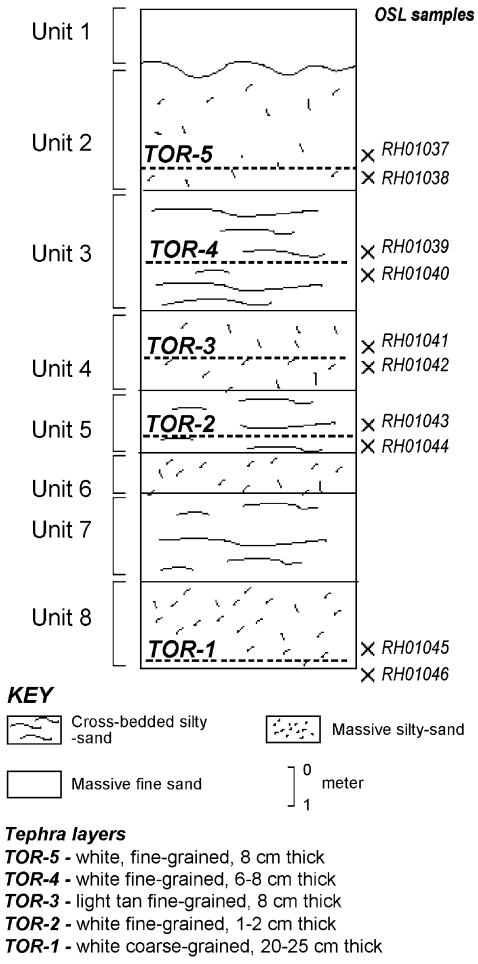

Fig. 3. Log of section at Las Torrecitas showing location of the tephra layers (TOR-1 to -5) and optical dating samples (RH01037–RH01046).

whether there was significant internal geochemical variation within a morphologically uniform unit. Two tephra layers were sampled at the final site, Puente Roto (Figs. 2b and 4). During earlier fieldwork, two optical dating samples had been obtained either side of the uppermost tephra here as part of a successful pilot study to determine whether the age of the alluvial sediments could be reliably determined using the optically stimulated luminescence (OSL) of fine-silt-sized quartz.

Methodology

Luminescence dating

Dating of tephra directly by luminescence methods requires the extraction and isolation of volcanic glass (Berger and Huntley, 1983, 1994), xenolithic quartz (Li and Yin, 2001), or volcanogenic quartz (Bonde et al., 2001; Li and Yin, 2001). Optical dating of fine-silt-sized glass is often problematic, resultant of a weak luminescence signal (Berger and Huntley, 1994; Berger and Neill, 1999) and intersample variation in spectral response (Berger and Neill, 1999). The use of volcanogenic quartz has been limited due either to its scarcity in andesitic and rhyodacitic tephra, or to its absence in tephra deposited at sites distal from the source (Fisher and Schminke, 1984). Problems have arisen even when quartz isolation techniques have apparently been successful. Bonde et al. (2001), for instance, reported vast age underestimates as well as significant fading of OSL on laboratory timescales. Li and Yin (2001) noted, in using the predose technique (Fleming, 1973), that xenolithic quartz provided accurate age estimates, while volcanogenic quartz yielded age reversals.

In view of the potential problems and degree of technical development required for dating tephra directly, it was decided in the present study to date the alluvial sediments immediately to either side of tephra units in order to constrain the age of each layer. Fine silt grains of quartz were isolated and their OSL was measured, as opposed to the conventional use of polymineral samples for this grain size, to avoid the possibility of age underestimates attributable to anomalous fading of feldspars (Wintle, 1973) within the polymineral fraction.

Block samples (100 × 100 × 75 mm) were collected for optical dating from the alluvial deposits on either side of each of the five tephra layers at Las Torrecitas (OSL samples RH01037-RH01046; Figs. 3 and 4). The samples were then transported to the laboratory and processed under controlled lighting conditions. Subsequent to the removal of the outer layer exposed to sunlight during sample collection, the blocks were dried at 40°C. Sample block RH01038 collapsed on opening and, due to potential contamination by material exposed to light during collection, was omitted from further study. Sedimentation of the <90 μm fraction in a 10 cm column of acetone facilitated the isolation of (5–15 μm) quartz grains and other mineral grains of varying density and size. Further pretreatments included immersion in 10% HCl to dissolve carbonate materials, while feldspars and amorphous silica were removed from the remaining fraction through digestion in 35% H_2SiF_6 for 2 weeks (Berger et al., 1980; Jackson et al., 1976). Following addition of 10% HCl to remove acid soluble fluorides, grains degraded to <5 μm as a result of acid pretreatment were removed by acetone sedimentation. A minimum of six aliquots (ca. 1.5 mg) were mounted on aluminium discs.

The measurement of luminescence from these aliquots was made using an automated TL-DA-12 Risø set. Blue light-emitting diodes, whose output was filtered by a 3 mm Schott GG420 (Bøtter-Jensen et al., 1999), were used as the stimulating light source. The wavelength of stimulating photons was 470Δ80 nm at a power of 15 $mWcm^{-2}$. Infrared stimulation, provided by IR diodes, was used to indicate the presence of contaminant feldspars (Hütt et al., 1988)—no such contamination was detected using this diagnostic. Photon emissions from each aliquot were filtered by three 2.5 mm HOYA U-340 and detected by a blue-green

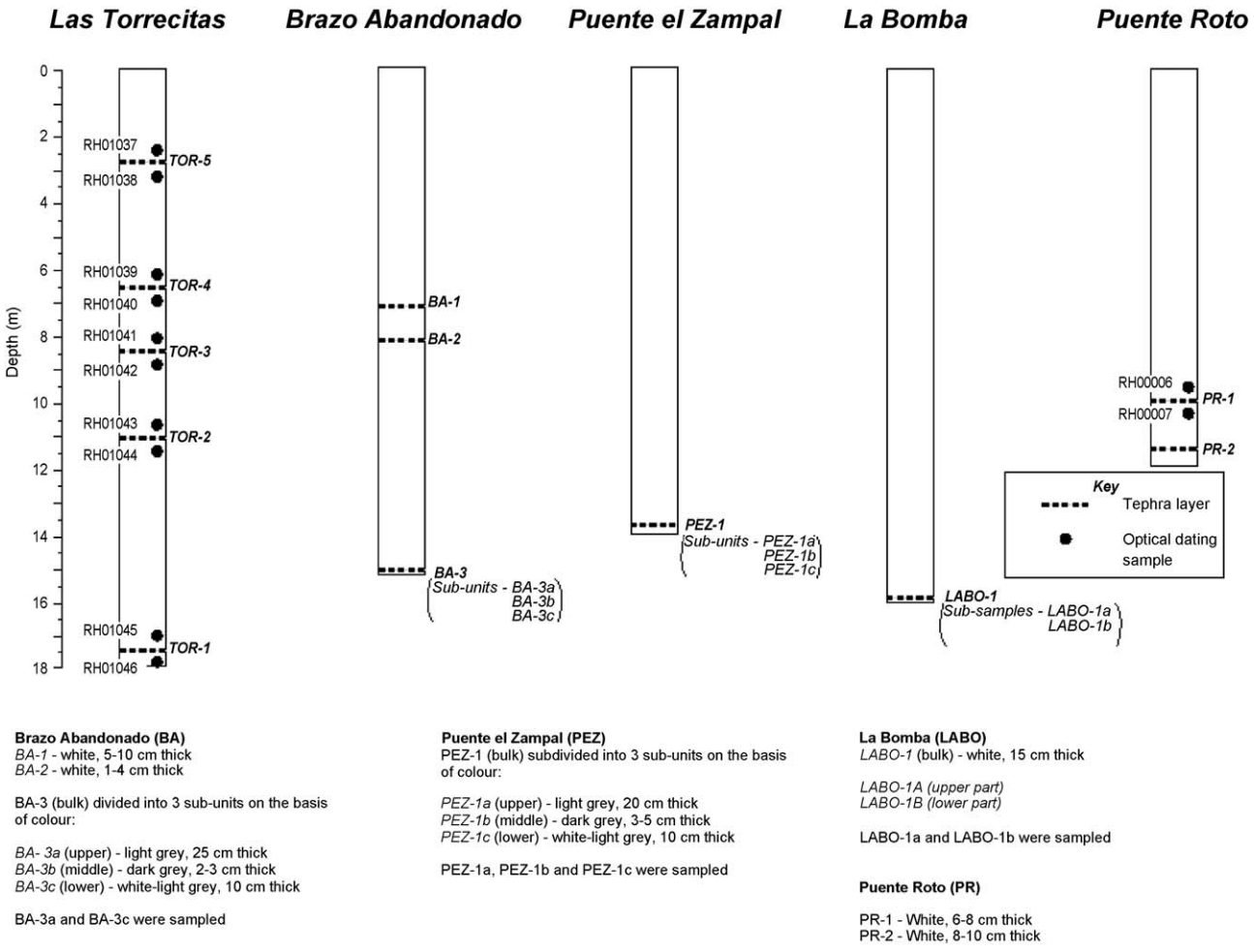

Fig. 4. Summary log indicating position of tephra layers and optical dating samples at the five study sites.

sensitive (EMI 9235QA) photomultiplier fitted with a bialkali photocathode. Natural luminescence signals were calibrated using regenerative-doses administered by a $^{90}Sr/^{90}Y$ beta source, itself calibrated for 5–15 μm quartz against the 'Hotspot 800' ^{60}Co gamma source located at the National Physical Laboratory, UK.

Equivalent dose (D_e) estimates were made using a modified version of the single-aliquot regenerative-dose (SAR) protocol proposed by Murray and Wintle (2000). Up to six different regenerative doses were given so as to define a linear portion of the dose response curve from each aliquot. The D_e value and associated error for each aliquot was then obtained by interpolation from laboratory dose response fitted using linear regression (Green and Margerison, 1978). A preheat of 260°C for 10 s was employed prior to the measurement of the natural and regenerated luminescence. The OSL response to a test dose of 5 Gy, preheated at 180°C for 10 s, was used to monitor and correct for the change in sensitivity throughout the measurement of natural and regenerated luminescence. Optical stimulation of each aliquot occurred at 160°C in order to reduce the effects of phototransferred thermoluminescence. The weighted mean D_e value obtained from aliquots of each sample was calculated.

In situ measurements of gamma contributions to each sample emitted through the radioactive decay of U, Th, and K in the surrounding sediment were made using an EG&G MicroNOMAD portable NaI gamma spectrometer. The spectrometer was calibrated against the standard blocks of U, Th, and K housed at RLAHA, University of Oxford, UK. Neutron Activation Analysis (NAA), provided by Becquerel Laboratories, Australia, was performed on subsamples from each block in order to determine the local alpha and beta contributions of U, Th, and K. Dose-rate calculations, based upon the methodology described by Aitken (1985), incorporated dose-rate conversion factors outlined by Adamiec and Aitken (1998) and the absorption coefficient for water content (Zimmerman, 1971) present in each sample, attaching a 25% relative uncertainty in an attempt to accommodate the effects of potential variations in past moisture content. The a-value for each sample was assumed to be 0.050 ± 0.002, premised upon a mean a-value directly assessed from 23 samples collected from loess–paleosol sequences across Argentina (Toms, unpublished). Estima-

Table 1
Electron microprobe analytical conditions and standards

Element	Counting time (seconds)		Standards
	Peak	Background	
Na[a]	10	MAN[b]	CCNM-211 obsidian
Mg	10	5	NIST K-411 glass
Al	10	MAN	CCNM-211 obsidian
Si	10	MAN	CCNM-211 obsidian
Fe	60	20	VG-A99 glass
Ca	22	7	NIST K-411 glass
Ti	22	7	Sphene 1A
K	30	MAN	CCNM-211 obsidian
Cl	30	7	KCl

Note. All elements analyzed using *K*α spectra.
[a] Acceleration voltage 15 kV, beam current 20 nA, beam diameter 8 μm.
[b] Background calculated using mean atomic number of sample.

tions of cosmic dose were made following the method outlined by Prescott and Hutton (1994). Luminescence ages were obtained by dividing the D_e value by the total dose rate value. The error in luminescence age estimates is quoted at 1σ confidence and is premised upon the propagation of both systematic and experimental (1σ) errors associated with those parameters, outlined above, contributing to the calculation of D_e and dose rate values.

Electron microprobe

Several hundred milligrams of each tephra were placed in shallow 8 mm glass rings glued to a standard petrographic slide. The rings, four to a slide, were then filled with a few drops of thermo-setting epoxy. After curing, the sample rings were trimmed with a low speed diamond micro-saw to a uniform thickness, and then polished using 1200 alumina grit followed by a 1 μm diamond paste. After carbon coating the glass shards (>20 μm) that appeared homogeneous at 400× under transmitted light were analyzed using a Cambax™ EMP in the GeoAnalytical Laboratory of the Department of Geology, Washington State University. The instrumental conditions and standards used are given in (Table 1).

Results and discussion

The geochemical similarity between glasses in individual tephra layers was compared using the similarity coefficient of Borchardt et al. (1972) as a discriminator (Begét et al., 1997; Benson et al., 1997; Hallett et al., 2001; King et al., 2001). Unit weighting was given to the oxides of Fe, Ca, K, Si, and Al and 0.25 weighting to those of Ti and Mg due to the low content of these elements and the consequent potential for minor analytical error to result in high relative error of their measured content (Hallett et al., 2001; King et al., 2001; Rieck et al., 1992). A weighting of 0.25 was also given to Na because of its high mobility in depositional environments and variations in concentration due to differing analytical conditions (Madsen et al., 2002). A similarity coefficient for two identical analyses would be 1.00. In the present study, a similarity coefficient of 0.95 or greater between two samples is taken to be suggestive of a correlation, provided that this is stratigraphically reasonable and that any supplemental geological information is in agreement (Busacca et al., 1992; Hallett et al., 2001; Sarna-Wojcicki and Davis, 1991).

Tephra geochemistry and luminescence-based chronology at Las Torrecitas

The EMP analysis indicates each tephra is a silica-rich rhyolite. EMP analysis of the glass in TOR-5 indicates that

Table 2
EMP data and similarity coefficients for glass shards within tephras at Las Torrecitas

Tephra	SiO_2 %	Al_2O_3 %	Fe_2O_3 %	TiO %	Na_2O %	K_2O %	MgO %	CaO %	Cl %	Number of analyses	Analytical total
TOR-5	77.46	13.06	0.91	0.16	3.10	4.30	0.13	0.75	0.13	20	94.72
	0.50	*0.27*	*0.10*	*0.03*	*0.16*	*0.11*	*0.03*	*0.07*	*0.02*		*0.89*
TOR-4	72.11	15.53	1.91	0.32	5.13	3.27	0.36	1.17	0.20	21	95.70
	0.25	*0.11*	*0.05*	*0.03*	*0.22*	*0.11*	*0.03*	*0.11*	*0.02*		*0.92*
TOR-3	72.7	15.17	1.87	0.32	4.68	3.3	0.4	1.39	0.17	20	96.16
	0.30	*0.17*	*0.08*	*0.02*	*0.12*	*0.11*	*0.03*	*0.08*	*0.02*		*0.70*
TOR-2	72.06	14.75	2.30	0.46	4.20	4.48	0.37	1.20	0.18	26	95.39
	0.31	*0.12*	*0.08*	*0.03*	*0.16*	*0.12*	*0.03*	*0.04*	*0.02*		*0.63*
TOR-1	72.83	14.81	1.85	0.32	4.11	4.38	0.32	1.19	0.19	20	95.18
	0.49	*0.49*	*0.28*	*0.06*	*0.24*	*0.38*	*0.08*	*0.25*	*0.02*		*0.71*
TOR-5		1.00									
TOR-4		0.71		1.00							
TOR-3		0.70		0.95		1.00					
TOR-2		0.73		0.89		0.87		1.00			
TOR-1		0.76		0.93		0.91		0.94		1.00	
Tephra layers		*TOR-5*		*TOR-4*		*TOR-3*		*TOR-2*		*TOR-1*	

Note. All analyses are normalized to 100 wt. %. Standard deviation of each analysis is given in italics.

this tephra layer has a well-constrained and unique geochemistry in comparison to TOR-1 to TOR-4, with similarity coefficients to these stratigraphically lower tephras ranging between 0.73 and 0.78 (Table 2). However, a similarity coefficient of 0.95 indicates that TOR-3 has a comparable geochemistry to TOR-4 (Table 2). Such geochemical equivalence occurs to a lesser extent between TOR-2 and TOR-1, with a similarity coefficient of 0.94. Nevertheless, it is noted that a significant difference exists between the contents of Ca within TOR-3 and TOR-4 and Fe in TOR-1 and TOR-2; therefore distinction on a compositional basis is feasible.

The optical ages of the samples bracketing each of the tephra layers at Las Torrecitas are shown in Table 3. The mean ages of RH01045 and RH01046 (bracketing TOR-1) appear to be reversed, whilst the upper mean age of TOR-3 (RH01041) is slightly younger than the lower mean age estimate for TOR-4 (RH01040). In both cases, however, associated errors suggest that the ages are statistically indistinguishable. The optical dating approach taken here is insufficiently precise to provide a statistically rigorous chronological differentiation between TOR-4 and TOR-3. The five tephras appear to have been deposited over a relatively short period of time spanning ca. 24,000 and 48,000 yr.

Tephra geochemistry at other sites

The geochemical similarity of subunit samples from BA-3 and also from PEZ-1 (Table 4) suggest that the color layering of these tephra observed in the field relate to postdepositional redox processes rather than accumulation of tephras from different eruptions or source volcanoes. In addition, the comparatively well-constrained geochemistry of these layers, indicated by the low standard deviations for individual analyses, suggest that these postdepositional processes had a negligible influence on shard geochemistry. The subunits of LABO-1 are also geochemically similar (Table 4), supporting the designation of the tephra layer as a single unit. On the basis of these results, only the mean compositions of PEZ-1, BA-3, and LABO-1 were used for geochemical comparison (Table 5) and correlation of tephra layers between sites (Table 6).

The geochemistry for the uppermost tephra layers BA-1 at Brazo Abandonado and PR-1 at Puente Roto are well constrained. In contrast, there are higher standard deviations associated with the individual elements for BA-2 and PR-2 (BA-2 bulk and PR-2 bulk: Table 5). Closer examination of the data indicates that each of these layers exhibits a bimodal geochemical composition (Fig. 5) with two distinct populations of volcanic glass (glass 1 and glass 2: Table 6). The composition of glass within tephra layers occasionally varies significantly in either a continuous or polymodal fashion (Davies et al., 2001; Dugmore et al., 1992). Most of this variation has been explained either by (1) physical mixing of tephras

Table 3
Dose rate, equivalent dose (D_e), and optical ages obtained for samples from Las Torrecitas (RH01037–RH01046: Figs. 3 and 4)

Tephra layer	Sample	NaI γ-spectrometery (in situ)			Total γ dose rate ($Gy.10^{-3}yr$)	Neutron activation analysis			Total α dose rate ($Gy.10^{-3}yr$)	Total β dose rate ($Gy.10^{-3}yr$)	Cosmic dose rate ($Gy.10^{-3}yr$)	Total dose rate ($Gy.10^{-3}yr$)	D_e (Gy)	Age (yr)
		K (%)	Th (ppm)	U (ppm)		K (%)	Th (ppm)	U (ppm)						
TOR-5	RH01037	2.08 ± 0.03	11.70 ± 0.30	3.54 ± 0.14	1.46 ± 0.02	2.40 ± 0.12	13.20 ± 0.66	3.31 ± 0.17	0.74 ± 0.03	2.63 ± 0.10	0.17 ± 0.02	4.99 ± 0.11	120.5 ± 4.9	24,100 ± 1100
	RH01038	1.79 ± 0.03	8.89 ± 0.27	2.70 ± 0.12	1.16 ± 0.02	2.44 ± 0.12	11.30 ± 0.57	2.64 ± 0.13	0.59 ± 0.03	2.45 ± 0.11	0.14 ± 0.01	4.34 ± 0.11	-	-
TOR-4	RH01039	1.76 ± 0.03	8.51 ± 0.25	2.79 ± 0.12	1.15 ± 0.02	2.06 ± 0.10	10.80 ± 0.54	3.09 ± 0.15	0.60 ± 0.03	2.16 ± 0.10	0.09 ± 0.01	4.00 ± 0.11	118.8 ± 7.3	29,700 ± 2000
	RH01040	1.75 ± 0.03	9.07 ± 0.25	2.39 ± 0.11	1.13 ± 0.02	2.12 ± 0.11	11.60 ± 0.58	2.75 ± 0.14	0.57 ± 0.03	2.13 ± 0.11	0.08 ± 0.01	3.92 ± 0.12	122.6 ± 6.8	31,300 ± 2000
TOR-3	RH01041	1.88 ± 0.03	8.53 ± 0.24	2.52 ± 0.11	1.15 ± 0.02	2.30 ± 0.12	10.40 ± 0.52	3.14 ± 0.16	0.58 ± 0.03	2.27 ± 0.12	0.07 ± 0.01	4.07 ± 0.12	122.3 ± 6.5	30,000 ± 1800
	RH01042	1.84 ± 0.03	9.46 ± 0.30	2.69 ± 0.14	1.20 ± 0.02	1.99 ± 0.10	11.20 ± 0.56	3.04 ± 0.15	0.60 ± 0.03	2.09 ± 0.10	0.07 ± 0.01	3.96 ± 0.11	132.8 ± 7.4	33,500 ± 2100
TOR-2	RH01043	2.01 ± 0.03	9.74 ± 0.26	3.14 ± 0.12	1.31 ± 0.02	2.92 ± 0.15	12.80 ± 0.64	3.51 ± 0.18	0.72 ± 0.03	2.96 ± 0.13	0.05 ± 0.01	5.04 ± 0.13	187.9 ± 9.3	37,200 ± 2100
	RH01044	1.97 ± 0.02	10.00 ± 0.23	2.98 ± 0.11	1.29 ± 0.02	2.25 ± 0.11	12.00 ± 0.60	3.33 ± 0.17	0.69 ± 0.03	2.45 ± 0.10	0.05 ± 0.01	4.48 ± 0.10	184.3 ± 8.0	41,200 ± 2000
TOR-1	RH01045	2.19 ± 0.02	11.69 ± 0.21	3.28 ± 0.10	1.46 ± 0.02	2.75 ± 0.14	14.40 ± 0.72	3.67 ± 0.18	0.76 ± 0.04	2.85 ± 0.13	0.03 ± 0.00	5.10 ± 0.13	252.6 ± 10.8	49,500 ± 2500
	RH01046	2.25 ± 0.03	12.28 ± 0.30	3.56 ± 0.13	1.52 ± 0.02	2.77 ± 0.14	15.40 ± 0.77	4.32 ± 0.22	0.83 ± 0.05	2.89 ± 0.15	0.03 ± 0.00	5.26 ± 0.15	247.7 ± 9.7	47,100 ± 2300

Table 4
EMP data and similarity coefficient for glass separates within subunits of tephra layers PEZ-1 (Puente El Zampal), BA-3 (Brazo Abandonado), and LABO-1 (La Bomba) indicated by suffix a, b, and/or c. Mean data are calculated from values generated from glass within the subunits

Tephra	SiO_2 %	Al_2O_3 %	Fe_2O_3 %	TiO %	Na_2O %	K_2O %	MgO %	CaO %	Cl %	Number of analyses	Analytical
					BA-3 (Brazo Abandonado 3)						
BA-3 (mean)	73.24	15.56	2.14	0.33	3.84	3.17	0.36	1.16	0.20	40	
	0.33	*0.17*	*0.07*	*0.02*	*0.28*	*0.08*	*0.03*	*0.07*	*0.02*		
BA-3a	73.2	15.56	2.13	0.32	3.86	3.20	0.36	1.16	0.20	19	95.17
	0.30	*0.09*	*0.05*	*0.03*	*0.30*	*0.08*	*0.02*	*0.04*	*0.03*		*0.84*
BA-3b	73.27	15.56	2.15	0.33	3.83	3.13	0.36	1.17	0.20	21	95.29
	0.36	*0.22*	*0.08*	*0.02*	*0.26*	*0.06*	*0.04*	*0.09*	*0.02*		*0.52*
					PEZ-1 (Puente El Zampal 1)						
PEZ-1 (mean)	73.04	15.76	2.12	0.33	3.78	3.20	0.37	1.19	0.20	52	
	0.22	*0.14*	*0.06*	*0.03*	*0.22*	*0.07*	*0.02*	*0.04*	*0.02*		
PEZ-1a	73.17	15.66	2.14	0.32	3.74	3.23	0.37	1.18	0.20	17	95.24
	0.21	*0.15*	*0.05*	*0.03*	*0.25*	*0.07*	*0.02*	*0.04*	*0.02*		*0.65*
PEZ-1b	73.04	15.78	2.11	0.33	3.77	3.18	0.37	1.21	0.21	17	95.07
	0.14	*0.07*	*0.07*	*0.02*	*0.13*	*0.08*	*0.02*	*0.03*	*0.02*		*0.52*
PEZ-1c	72.93	15.85	2.11	0.33	3.84	3.20	0.37	1.18	0.20	18	95.16
	0.23	*0.12*	*0.05*	*0.03*	*0.25*	*0.06*	*0.02*	*0.04*	*0.02*		*0.67*
					LABO-1 (La Bomba 1)						
LABO-1 (mean)	72.88	15.55	2.09	0.33	4.19	3.22	0.36	1.17	0.20	39	
	0.39	*0.17*	*0.04*	*0.02*	*0.27*	*0.08*	*0.02*	*0.05*	*0.02*		
LABO 1a	72.98	15.47	2.10	0.32	4.16	3.24	0.36	1.16	0.20	19	95.59
	0.44	*0.20*	*0.05*	*0.02*	*0.25*	*0.08*	*0.02*	*0.05*	*0.02*		*0.73*
LABO 1b	72.78	15.62	2.09	0.33	4.21	3.21	0.37	1.18	0.21	20	95.39
	0.32	*0.09*	*0.04*	*0.02*	*0.29*	*0.07*	*0.02*	*0.06*	*0.02*		*0.77*
					BA-3: similarity coefficients between bulk and subunit composition						
BA-3 (mean)		1.00									
BA-3a		1.00			1.00						
BA-3b		1.00			0.99			1.00			
Tephra layers		*BA-3 (mean)*			*BA-3a*			*BA-3b*			
					PEZ-1: similarity coefficients between bulk and subunit composition						
PEZ-1 (mean)		1.00									
PEZ-1a		0.99			1.00						
PEZ-1b		0.99			0.99			1.00			
PEZ-1c		1.00			0.99			0.99		1.00	
Tephra layers		*PEZ-1 (mean)*			*PEZ-1a*			*PEZ-1b*		*PEZ-1c*	
					LABO-1: similarity coefficients between bulk and subunit composition						
LABO-1 (mean)		1.00									
LABO-1a		1.00			1.00						
LABO-1b		1.00			0.99			1.00			
Tephra layers		*LABO-1 (mean)*			*LABO-1a*			*LABO-1b*			

Note. All analyses are normalized to 100 wt. %. Standard deviation of each analysis given is in italics.

from more than one source during deposition (simultaneous eruptions) or postdepositional reworking (Kvamme et al., 1989), (2) incorporation of preexisting volcanic deposits from around the vent during the eruption (Hooper et al., 1980), and (3) eruption of a stratified/chemically zoned magma or mixed magmas (Carey and Sigurdsson, 1978; Carr and Walker, 1987; Stokes and Lowe, 1988). The lack of evidence of reworking or stratification of these layers within the field, and the absence of lithic fragments under the microscope suggest that the bimodal glass composition of BA-2 and PR-2 is due to the erupting source volcano(s) having a mixed or chemically zoned magma chamber.

Intersite geochemical correlation of tephra layers

TOR-5, BA-1, and PR-1 are geochemically indistinguishable from one another and thus are considered equivalent (Table 6, Fig. 6). Further support for the correlation of PR-1 and TOR-5 is provided by the optical dates bracketing PR-1, namely 22,300 ± 1900 yr (RH00006) and 24,900 ± 2500 yr (RH00007) (Table 7). These ages are

Table 5
EMP data and similarity coefficient for glass separates of tephra at Brazo Abandonado, Puente el Zampal, La Bomba, and Puente Roto: *combined* values reflect analysis of bulk glass composition, and *Glass 1* and *Glass 2* values relate to data obtained from glass shards of one of two distinct populations (Fig. 5)

Tephra	SiO_2 %	Al_2O_3 %	Fe_2O_3 %	TiO %	Na_2O %	K_2O %	MgO %	CaO %	Cl %	Number of analysis	Analytical total
Brazo Abandonado (BA)											
BA-1	77.55	12.89	0.96	0.17	2.98	4.47	0.13	0.73	0.13	21	94.31
	0.56	*0.32*	*0.10*	*0.02*	*0.19*	*0.28*	*0.03*	*0.07*	*0.01*		*0.97*
BA-2 (combined)	71.92	14.71	2.67	0.46	3.46	4.15	0.58	1.91	0.16	23	95.56
	3.72	*1.14*	*1.11*	*0.0*	*0.06*	*0.62*	*0.41*	*0.96*	*0.04*		*1.71*
Two discrete geochemical populations (Glass 1 and Glass 2) identified within BA-2											
Glass 1	74.62	13.93	1.85	0.30	3.06	4.56	0.29	1.21	0.17	15	94.40
	1.02	*0.46*	*0.44*	*0.06*	*0.24*	*0.39*	*0.11*	*0.30*	*0.04*		*0.63*
Glass 2	67.12	16.16	3.87	0.71	4.20	3.58	1.10	3.13	0.13	8	97.58
	0.86	*0.22*	*0.26*	*0.04*	*0.23*	*0.14*	*0.15*	*0.26*	*0.02*		*1.06*
BA-3 (mean)	73.24	15.56	2.14	0.33	3.84	3.17	0.36	1.16	0.20	40	95.17
	0.33	0.17	0.07	0.02	0.28	0.08	0.03	0.07	0.02		0.84
Puente Roto (PR)											
PR-1	77.39	13.18	0.95	0.16	2.79	4.48	0.14	0.76	0.14	21	93.94
	0.61	*0.33*	*0.10*	*0.03*	*0.25*	*0.26*	*0.03*	*0.08*	*0.02*		*0.92*
PR-2 (combined)	68.76	15.90	3.50	0.62	3.44	3.81	0.96	2.85	0.15	24	95.09
	3.49	*1.08*	*1.04*	*20*	*0.55*	*0.49*	*0.39*	*0.93*	*0.03*		*1.78*
Two discrete geochemical populations (Glass 1 and Glass 2) identified within layer PR-2											
Glass 1	73.8	14.36	2.00	0.33	2.90	4.52	0.39	1.52	0.18	7	93.81
	1.59	*0.71*	*0.50*	*0.09*	*0.13*	*0.27*	*0.13*	*0.42*	*0.02*		*0.47*
Glass 2	66.68	16.53	4.12	0.74	3.66	3.53	1.20	3.40	0.14	17	95.57
	0.95	*0.22*	*0.27*	*0.04*	*0.50*	*0.13*	*0.12*	*0.27*	*0.02*		*1.87*
Puente El Zampal (PEZ)											
PEZ-1 (mean)	73.04	15.76	2.12	0.33	3.78	3.20	0.37	1.19	0.20	52	
	0.22	*0.14*	*0.06*	*0.03*	*0.22*	*0.07*	*0.02*	*0.04*	*0.02*		
La Bomba (LABO)											
LABO-1 (mean)	72.88	15.55	2.09	0.33	4.19	3.22	0.36	1.17	0.20	39	
	0.39	*0.17*	*0.04*	*0.02*	*0.27*	*0.08*	*0.02*	*0.05*	*0.02*		

Note. All analyses are normalized to 100 wt. %. Standard deviation for each analysis is given in italics.

Table 6
Similarity coefficients expressing the geochemical correspondence between tephra layers: similarity coefficients >0.95, indicating tephra layers that are correlatives of each other, are shown in bold

TOR-1	1.00																
TOR-2	0.94	1.00															
TOR-3	0.91	0.87	1.00														
TOR-4	0.93	0.89	**0.95**	1.00													
TOR-5	0.76	0.73	0.70	0.71	1.00												
BA-1	0.78	0.74	0.69	0.70	**0.97**	1.00											
BA-2	0.83	0.88	0.82	0.80	0.68	0.68	1.00										
BA-2 glass 1	**0.96**	0.93	0.88	0.89	0.78	0.79	0.82	1.00									
BA-2 glass 2	0.69	0.72	0.73	0.72	0.57	0.57	0.79	0.66	1.00								
BA-3	0.91	0.90	0.93	**0.96**	0.70	0.70	0.81	0.88	0.72	1.00							
PEZ-1	0.91	0.91	0.93	**0.96**	0.70	0.69	0.81	0.88	0.73	**0.99**	1.00						
LABO-1	0.91	0.91	0.94	**0.97**	0.70	0.70	0.81	0.88	0.73	**0.99**	**0.99**	1.00					
PR-1	0.77	0.75	0.70	0.71	**0.98**	**0.98**	0.68	0.70	0.57	0.70	0.70	0.70	1.00				
PR-2	0.72	0.75	0.74	0.73	0.61	0.60	0.84	0.72	0.93	0.74	0.74	0.74	0.60	1.00			
PR-2 glass 1	0.92	0.91	0.90	0.87	0.74	0.75	0.87	0.93	0.70	0.87	0.87	0.87	0.75	0.74	1.00		
PR-2 glass 2	0.67	0.69	0.71	0.70	0.56	0.56	0.77	0.65	**0.96**	0.71	0.71	0.71	0.56	0.90	0.68	1.00	
	TOR-1	**TOR-2**	**TOR-3**	**TOR-4**	**TOR-5**	**BA-1**	**BA-2**	**BA-2 glass 1**	**BA-2 glass 2**	**BA-3**	**PEZ-1**	**LABO-1**	**PR-1**	**PR-2**	**PR-2 glass 1**	**PR-2 glass 2**	

Note. Similarity coefficients calculated using unit weighting for oxides except Na_2O, TiO, and MgO, weighted by 0.25.

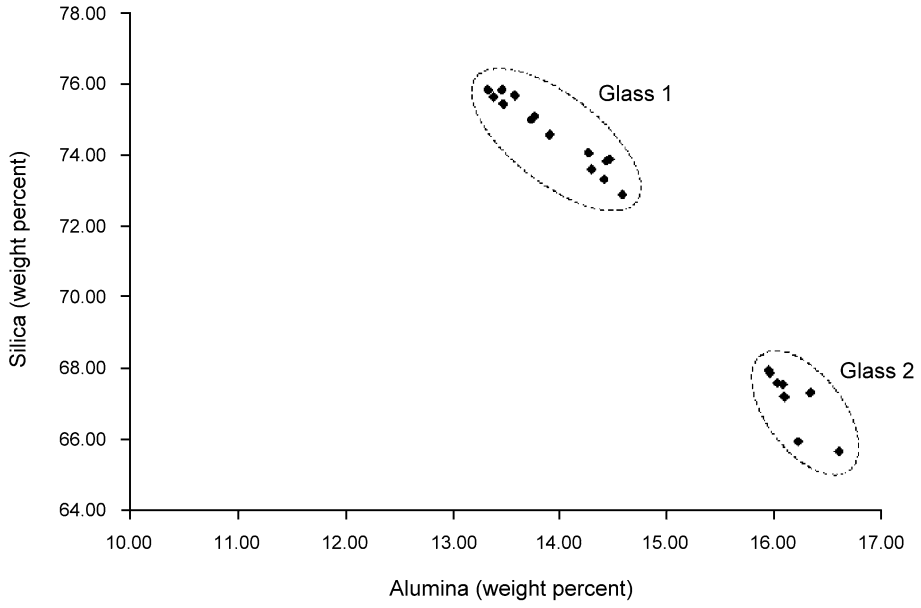

Fig. 5. Silica–alumina content of Glass 1 and Glass 2 in BA-2 (Brazo Abandonado).

concordant with the optical date of 24,200 ± 1100 yr obtained just above TOR-5 (Table 3). It is noted that the optical dates from Puente Roto are compatible with a conventional radiocarbon age of 10,090 ± 50 yr BP (Beta-154136) for a paleosol 4.5 m above the level of PR-1.

TOR-4, BA-3, PEZ-1, and LABO-1 have also been correlated on the basis of high similarity coefficients (0.96–0.99; Table 6, Fig. 6). Their correlation enables the basal part of the sections at Brazo Abandonado, Puente el Zampal, and La Bomba to be dated to approximately 30,000 yr, the mean optically dated age of TOR-4. This maximum

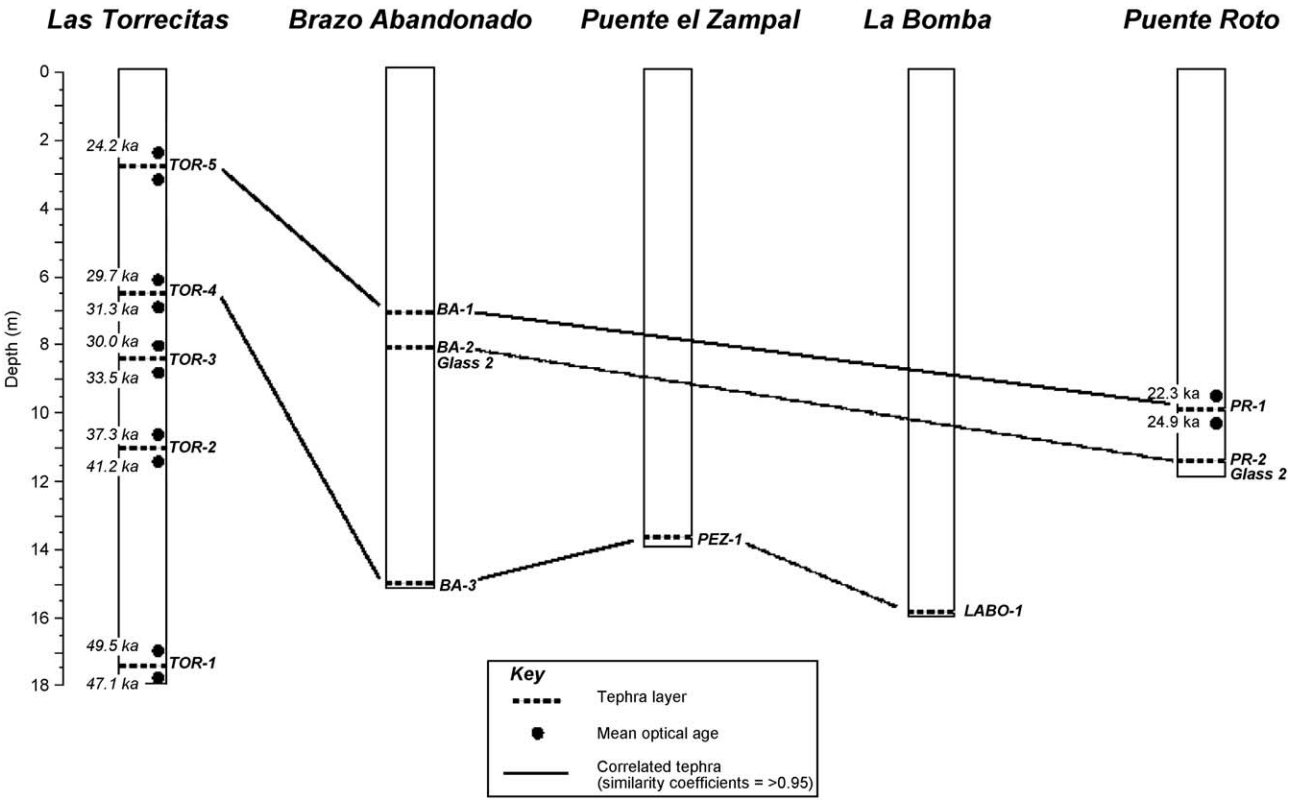

Fig. 6. Optical ages and correlation of tephras between study sites.

Table 7
Dose rate, equivalent dose (D_e), and optical age data obtained for samples from Puente Roto (RH00006–RH00007: Figs. 4 and 6)

Tephra layer	Sample	NaI γ-spectrometry (in situ)			Total γ dose rate ($Gy.10^{-3}yr$)	Neutron activation analysis			Total α dose rate ($Gy.10^{-3}yr$)	Total β dose rate ($Gy.10^{-3}yr$)	Cosmic dose rate $2(Gy.10^{-3}yr)$	Total dose rate ($Gy.10^{-3}yr$)	D_e (Gy)	Age (yr)
		K (%)	Th (ppm)	U (ppm)		K (%)	Th (ppm)	U (ppm)						
PR-1	RH00006	1.98 ± 0.03	9.84 ± 0.30	2.71 ± 0.13	1.26 ± 0.02	2.00 ± 0.10	11.60 ± 0.58	2.32 ± 0.12	0.49 ± 0.02	2.15 ± 0.08	0.05 ± 0.01	3.94 ± 0.09	87.9 ± 6.4	22,300 ± 1700
	RH00007	1.94 ± 0.03	9.03 ± 0.28	2.41 ± 0.12	1.17 ± 0.02	2.15 ± 0.11	10.80 ± 0.54	2.29 ± 0.11	0.42 ± 0.02	2.19 ± 0.09	0.04 ± 0.01	3.83 ± 0.09	95.4 ± 8.7	24,900 ± 2400

age for the section is not in conflict with a radiocarbon date of 17,110 ± 70 yr BP (Beta-154137) (Zárate, 2002) obtained from organic material within a thin paleosol located 4 m above the tephra at Puente el Zampal. It is noted that while the glass in TOR-3 is similar to that in TOR-4, its geochemistry is relatively distinct from BA-3, PEZ-1, and LABO-1, suggesting that equivalence of these three tephra to TOR-4 is more probable.

A similarity coefficient of 0.96 is denoted in Table 6 between TOR-1 and BA-2 glass 1. If these tephra do relate to the same eruption then the implication is that tephras equivalent of TOR-2 to TOR-4 are not found at other sites in this study. This would conflict with the correlation described above of TOR-4 to BA-3, PEZ-1, and LABO-1. The principal geochemical case against TOR-1 and BA-2 glass 1 being isochronous is the lack of a bimodal glass population within TOR-1 compared to BA-2, previously ascribed herein to an eruption from a mixed or chemically zoned magma chamber.

PR-2 and BA-2 are tentatively correlated as they each exhibit a distinct bimodal geochemical composition with high similarity coefficients (0.96; Table 6, Fig. 6) between one of the glasses (PR-2, glass 2, and BA-2, glass 2) in both of these layers. Moreover, their correlation is consistent with their stratigraphic position in relation to the overlying BA-1 and PR-1 correlatives (Fig. 6). The similarity coefficient between the other glass subpopulation (PR-2, glass 1, and BA-2, glass 1) in both layers is lower (0.93), but nonetheless notable. The relatively high standard deviations for individual oxides within glasses 1 and 2, reflects the degree of chemical variability within these layers. In view of the correlation of BA-3 and TOR-4 as well as BA-1 and TOR-5, it appears that BA-2 and PR-2 represent a tephra, associated with a volcanic eruption between ca. 24,000 and 30,000 yr, that is not visible at Las Torrecitas.

Supplemental evidence for correlation

It has been proposed that at least two eruptions represented by tephra layers at Las Torrecitas, TOR-4 and TOR-5, can be geochemically correlated with those at other sites. Support for this view and for the suggestion of differentiation between geochemically comparable type-site tephras (TOR-3 to TOR-4 and TOR-1 to TOR-2) on the basis of Ca and Fe contents, respectively, may be sought from supplemental tephrological data. Further, the extension of a tephrochronological framework founded upon this type site beyond the geographical limits of this study may benefit from such mineralogical, morphological, and textural evidence to enable confident correlation, although the limitations placed by gravitational sorting on the spatial consistency of these data should be borne in mind.

All of the tephras correlated on the basis of glass composition are morphologically and mineralogically sim-

ilar. All range from very fine to medium sand size (4 phi to 1 phi) and, with exception of BA-2 and PR-2, all are found in five of the stratigraphic units designated at the Torrecitas section (Fig. 3). The tephra descriptions are based on examination of oil immersion mounts using transmission microscopy and polished thin sections using transmission and reflection microscopy. Glass percentages and mineral proportions are based on visual estimates. No lithic fragments were observable.

Stratigraphic unit 2 hosts TOR-5, which is correlated to BA-1 and PR-1. These tephras are very similar in appearance with each consisting of approximately 95% small glass shards (<50 μm) with rare pumice (<200 μm in maximum dimension). The mineral proportions in each are quartz (Q) + feldspar (F) > biotite (B) > hornblende (Hbl) and the abundance of colorless glass shards and rarity of pumice give this tephra a white appearance.

Stratigraphic unit 3 incorporates tephra TOR-4 which is correlated to LABO-1a, 1b; PEZ-1a, 1b, 1c; BA-3a, 3b, 3c. The suffixes a, b, and c represent textural subunits (upper to lower) of the numbered beds. Each of the subunits is texturally and mineralogically similar to the corresponding subunit in the other stratigraphic sections. LABO-1a, PEZ-1a, and BA-3a consist of approximately 95% glass shards (averaging approximately 30 μm) and occasional microlite containing pumice up to 300 μm with Q + F > B > Hyp (hypersthene), but no amphibole observed. TOR-4, LABO-1b, PEZ-1b, and BA-3b contain less glass (~70%) and are much coarser with shards averaging 50 μm and altered microlite-containing pumice up to 500 μm. All contain large (<500 μm) mineral crystals, some of which are glass-coated, in the proportions Q + F ~ Hyp > Hbl > B. PEZ-1c and BA-3c contain 90% glass and are slightly coarser with more altered pumice (up to 300 μm) than subunit 1a samples. Mineral proportions are Q + F > Hyp with no amphibole being observed.

TOR-3 is housed within stratigraphic unit 4 and consists of approximately 85% glass shards averaging ~30 μm with abundant (20%), partly devitrified pumice containing Fe oxides and hypersthene crystals. The pumice and mineral crystals are up to 300 μm in maximum dimension and the inclusions in the pumice render a dirty appearance, which gives the tephra its overall light tan color. Mineral proportions are Q + F > B > Hyp ~ Hbl.

Therefore, complications in correlation induced by the geochemical similarity of TOR-4 to TOR-3 may, in addition to contemplation of Ca content, be circumvented if within each the contrast in mineral proportions, texture and inclusions are considered. The proportion of biotite is greater than that of hypersthene or hornblende within TOR-3, but occurs as the smallest proportion of minerals within TOR-4. TOR-4 also appears to have coarser glass, pumice, and mineral fractions than TOR-3. Finally, pumice within TOR-3 contains inclusions that generate a darker color contrasting with that of TOR-4.

Stratigraphic unit 5 contains tephra TOR-2. This tephra comprises approximately 80% glass shards averaging 50 μm and abundant pumice of two types: clear pumice (60%) with spherical and oval vesicles and a tan, microlite-filled and partially devitrified pumice (20%). The mineral proportions are Q + F > B > Hyp > Hbl.

Tephra TOR-1 within stratigraphic unit 8 is composed of approximately 85% clear glass shards and pumice with spherical to oval vesicles. The glass shards average ~80 μm maximum dimension with pumice and mineral crystals, some glass-coated, up to 500 μm. The mineral proportions are Q + F > Hyp > B > Hbl.

Given that tephra TOR-2 contains pumice of two types and TOR-1 only one, a diagnostic is available, in addition to the consideration of Fe concentrations, with which to distinguish these geochemically similar tephras. In addition, TOR-2 appears to comprise a greater proportion of biotite than hypersthene, with converse proportions of these mineral constituents within TOR-1.

The geochemical correlation of tephras BA-2 to PR-2, representing a volcanic event not registered at Las Torrecitas, is supported by each having a similar and distinctive mineral assemblage (Q + F > Hyp ~ Hbl > B), consisting of abundant and large (up to 300 μm) euhedral hypersthene, euhedral brown oxyhornblende, and minor biotite.

Conclusions

A total of six volcanic eruptions, occurring between ca. 24,000 and 48,000 yr, are chronicled by tephras within this study. Of these, two tephras (TOR-5 and BA-2/PR-2) deposited ca. 24,000 yr and between ca. 24,000 and 30,000 yr, respectively, have major oxide compositions sufficiently distinct for correlation premised upon geochemical similarity coefficients alone. This statistical measure of correspondence between tephras exercised here suggests the eruption at ca. 30,000 yr registered by TOR-4 is the oldest tephra traceable to other sites in this study. Representation by tephra of the remaining three eruptions at ca. 32,000, 39,000, and 48,000 years are restricted to the type-site Las Torrecitas.

Resemblance in major oxide structure of type-site tephras, TOR-1 with TOR-2 and TOR-3 with TOR-4, reflected by similarity coefficients of 0.94–0.95, does not preclude discrimination and hence correlation on geochemical grounds given the contrast in Fe and Ca contents, respectively. Distinction of these tephra pairs on a compositional basis is further supported by supplemental tephrological evidence. Indeed, all of the intersite correlations established at this juncture are fully substantiated by respective mineralogical, morphological and textural data.

This pilot study therefore provides a basis for the establishment of a local tephrochronological framework. Its extension beyond the alluvial sequences of central western Argentina is encouraged by the occurrence of

geochemically distinct tephra verified and dated in this study. Given the necessity of a firm chronostratigraphic foundation, required for reconstructing climate change from loess and alluvial sequences across central Argentina, the pursuit of a regional tephrochronological framework appears advisable.

Acknowledgments

We thank José Hernández for field assistance and James Smith for providing the base illustration for Fig. 1. This project was funded by the Royal Society (Grant 574006.G503/22258). Funding for Phillip Toms and Matthew King was provided by a research grant (F/07537A) from the Leverhulme Trust.

References

Adamiec, G., Aitken, M.J., 1998. Dose rate conversion factors: new data. Ancient TL 16, 37–50.

Aitken, M.J., 1985. Thermoluminescence Dating. Academic Press, London.

Auer, V., 1974. The isorhythmicity subsequent to the Fuego–Patagonian and Fenoscandian ocean level transgressions and regressions of the last glaciation. Annales Academia Scientiarum Fennicae Series A III 115, 1–188.

Begét, J.E., Keskinen, M.J., Severin, K.P., 1997. Tephrochronologic constraints on the Late Pleistocene history of the southern margin of the Cordilleran Ice Sheet, western Washington. Quaternary Research 47, 140–146.

Benson, L.V., Smoot, J.P., Michaele, K., Sarna-Wojcicki, A., Burdett, J.W., 1997. Radiocarbon ages and environments of deposition of the Wono and Trego Hot Springs tephra layers in the Pyramid Lake Subbasin, Nevada. Quaternary Research 47, 251–260.

Berger, G.W., Huntley, D.J., 1983. Dating volcanic ash by thermoluminescence. PACT 9, 581–592.

Berger, G.W., Huntley, D.J., 1994. Tests for optically stimulated luminescence from tephra glass. Quaternary Science Reviews (Quaternary Geochronology) 13, 509–512.

Berger, G.W., Mulhern, P.J., Huntley, D.J., 1980. Isolation of silt-sized quartz from sediments. Ancient TL 11, 147–152.

Berger, G.W., Neill, P.A., 1999. Photon-stimulated-luminescence (PSL) dating tests of glass-rich volcanic ash. Abstracts: LED99, 9th International Conference on Luminescence and Electron Spin Resonance Dating. Rome, p. 138.

Blasi, A., Zárate, M., Kemp, R., 2001. Sedimentación y pedogénesis cuaternaria en el noreste de la pampa bonaerense: la localidad Gorina como caso de estudio. Revista Argentina de Sedimentología 8 (1), 77–92.

Bonadonna, F.P., Leone, G., Zanchetta, G., 1995. Composición isotópica de los fósiles de gasterópodos continentales de la provincia de Buenos Aires. Indicaciones paleoclimáticas. In: Alberdi, M.T., Leone, G., Tonni, E.P. (Eds.), Un ensayo de correlación con el Mediterráneo occidental. Evolución biológica y climática de la región pampeana durante los últimos cinco millones de años. Monografías del Museo Nacional de Ciencias Naturales, Madrid, pp. 77–104.

Bonde, A., Murray, A.S., Friedrich, W.L., 2001. Santorini: Luminescence dating of a volcanic province using quartz? Quaternary Science Reviews (Quaternary Geochronology) 20, 789–793.

Borchardt, G.A., Aruscavage, P.J., Millard Jr., H.T., 1972. Correlation of Bishop Ash, a Pleistocene marker bed, using instrumental neutron activation analysis. Journal of Sedimentary Petrology 42, 301–306.

Bøtter-Jensen, L., Mejdahl, V., Murray, A.S., 1999. New light on OSL. Quaternary Science Reviews (Quaternary Geochronology) 18, 303–310.

Busacca, A.J., Nelstead, K.T., McDonald, E.V., Purser, M.D., 1992. Correlation of distal tephra layers in loess in the Channelled Scabland and Palouse of Washington State. Quaternary Research 37, 281–303.

Carey, S.N., Sigurdsson, H., 1978. Deep-sea evidence for distribution of tephra from the mixed magma eruption of Soufriere on St. Vincent, 1902: Ash turbidites and airfall. Geology 6, 271–274.

Carr, M.J., Walker, J.A., 1987. Intra-eruption changes in composition of some mafic to intermediate tephras from Central America. Journal of Volcanology and Geothermal Research 33, 147–159.

Clapperton, C., 1993. Quaternary geology and geomorphology of South America. Elsevier, Amsterdam, p. 779.

D'Antoni, H., 1983. Pollen analysis of Gruta del Indio. Quaternary of South America and Antarctic Peninsula 1, 83–104.

Davies, S.M., Branch, N.P., Lowe, J.J., Turney, C.S.M., 2002. Towards a European tephrochronological framework for Termination I and the early Holocene. Philosophical Transaction of the Royal Society of London Series A 360, 767–802.

Davies, S.M., Turney, C.S.M., Lowe, J., 2001. Identification and significance of a visible, basalt-rich Vedde Ash layer in a Late-glacial sequence on the Isle of Skye, Inner Hebrides, Scotland. Journal of Quaternary Science 16, 99–104.

Dugmore, A.J., Newton, A.J., Sugden, D.E., 1992. Geochemical stability of fine-grained silicic Holocene tephra in Iceland and Scotland. Journal of Quaternary Science 7, 173–183.

Fleming, S.J., 1973. The pre-dose technique: a new thermoluminescence dating method. Archaeometry 15, 13–30.

Fisher, R.V., Schminke, H.U., 1984. Pyroclastic Rocks. Springer-Verlag, New York.

Foit Jr., F.F., Mehringer, P.J., Sheppard, J.C., 1993. Age, Distribution and stratigraphy of Glacier Peak tephra in eastern Washington and western Montana, United States. Canadian Journal of Earth Sciences 30, 535–552.

González Bonorino, F., 1965. Mineralogía de las fracciones arcilla y limo del Pampeano en el área de la ciudad de Buenos Aires y su significado estratigráfico y sedimentológico. Asociación Geológica Argentina Revista 20, 67–148.

Green, J.R., Margerison, D., 1978. Statistical Treatment of Experimental Data. Elsevier Scientific, New York.

Gronvold, K., Oskarsson, N., Johnsen, S.J., Clausen, H.B., Hammer, C.U., Bond, G., Bard, E., 1995. Ash layers from Iceland in the Greenland GRIP ice core correlated with oceanic and land based sediments. Earth and Planetary Science Letters 54, 238–246.

Guerstein, G.R., 1993. Origen y Significado Geológico de la Asociación Piroclástica Pumícea. Pleistoceno de la Provinica de Mendoza entre los 33 30 y 34 40 L.S., tesis doctoral. Museo de la Plata.

Hallett, D.J., Mathewes, R.W., Foit Jr., F.F., 2001. Mid-Holocene Glacier Peak and Mount St. Helens We tephra layers detected in lake sediments from southern British Columbia using high-resolution techniques. Quaternary Research 55, 284–292.

Heusser, C.J., 1991. Biogeographic evidence for late Pleistocene palaeoclimate of Chile. Bamberger Geographische Schriften 11, 257–270.

Hildreth, W., Drake, R., 1992. Volcán Quizapu, Chilean Andes. Bulletin of Volcanology 54, 93–125.

Hildreth, W., Grunder, A.L., Drake, R.E., 1984. The Loma Seca Tuff and the Calabozos Caldera: a major ash flow and caldera complex in the Southern Andes of Central Chile. Petrochemistry and age of rhyolitic pyroclastic flows which occur along the drainage valleys of the Río Maipo and Río Cahapoal (Chile) and the Río Yaucha and Río Papagayos (Argentina). Revista Geológica de Chile, vol. 23, pp. 39–52.

Hooper, P.R., Herrick, I.W., Laskowski, E.R., Knowles, C.R., 1980. Composition of the Mt. St. Helens ashfall in the Moscow–Pullman Area on 18 May 1980. Science 209, 1125–1126.

Hütt, G., Jaek, I., Tchonka, J., 1988. Optical dating: K-feldspars optical response stimulation spectra. Quaternary Science Reviews 7, 381–386.

Inbar, M., Risso, C., 2001. A morphological and morphometric analysis of a high density cinder cone volcanic field-Payun Matru, southe central Andes, Argentina. Zeitschrift für Geomorphologie, None Folse 45 (3), 321–343.

Imbellone, P.A., Camilión, C., 1988. Characterization of a buried tephra layer in soils of Argentina. Pedologie 38, 155–171.

Iriondo, M., 1993. Geomorphology and Late Quaternary of the Chaco (South-America). Geomorphology 7, 289–303.

Iriondo, M., 1997. Models of deposition of loess and loessoids in the upper Quaternary of South America. Journal of South American Earth Sciences 10, 71–79.

Iriondo, M., 1999. The origin of silt particles in the loess question. Quaternary International 62, 3–9.

Iriondo, M., 2000. Patagonian dust in Antarctica. Quaternary International 68, 83–86.

Jackson, M.L., Sayin, M., Clayton, R.N., 1976. Hexafluorosilicic acid regent modification for quartz isolation. Soil Science Society of America Journal 40, 958–960.

Kemp, R.A., Zárate, M.A., 2000. Pliocene pedosedimentary cycles in the southern Pampas, Argentina. Sedimentology 47, 3–14.

King, M., Busacca, A.J., Foit Jr., F.F., Kemp, R.A., 2001. Identification of disseminated Trego Hot Springs tephra in the Palouse, Washington State. Quaternary Research 56, 165–169.

Kittl, E., 1933. Estudio sobre los fenómenos volcánicos y material caido durante la erupción del grupo del "Descabezado" en el mes be abril de 1932. Anal Museo Nacional Historica Naturale 37, 321–364.

Kraglievich, J.L., 1952. El perfil geológico de Chapadmalal y Miramar. Provincia de Buenos Aires. Revista Museo municipal Ciencias Naturales y Tradicionalista de Mar del Plata 1, 8–37.

Kröhling, D.M., 1999. Upper Quaternary geology of the lower Carcaraná Basin, North Pampa, Argentina. Quaternary International 57/58, 135–148.

Kukla, G., 1989. Long continental records of climate—an introduction. Palaeogeography, Palaeoclimatology, Palaeoecology 72, 1–9.

Kvamme, T., Mangerud, J., Furnes, H., Ruddiman, W.F., 1989. Geochemistry of Pleistocene ash zones in cores from the North Atlantic. Norsk Geologisk Tidsskrift 69, 251–272.

Larsson, W., 1937. Vulkanische Asche vom Ausbruch des Chile-nischen Vulkans Quizapu (1932) in Argentina gesammelt. Bulletin of the Geological Institution of the University of Upsala 26, 27–52.

Li, S.-H., Yin, G.-M., 2001. Luminescence dating of young volcanic activity in China. Quaternary Science Reviews (Quaternary Geochronology) 20, 865–868.

Madsen, D.B., Sarna-Wojcicki, A.M., Thompson, R.S., 2002. A late Pleistocene tephra layer in the southern Great Basin and Colorado plateau derived from Mono Craters, California. Quaternary Research 57, 382–390.

Markgraf, V., 1983. Late and postglacial vegetational and paleoclimatic changes in subantarctic, temperate and arid environments in Argentina. Palynology 7, 43–70.

Morrás, H., 1994. Descripción y caracterización análitica de depósitos piroclásticos en dos perfiles de suelo de la región chaqueña. Tucumán, Actas: V Reunión Argentina de Sedimentología, 165–170.

Muhs, D., Zárate, M., 2001. Late Quaternary eolian records of the Americas and their palaeoclimatic significance. In: Markgraf, V. (Ed.), Interhemispheric Climate Linkages. Academic Press, New York, pp. 183–216.

Murray, A.S., Wintle, A.G., 2000. Luminescence dating of quartz using an improved single-aliquot regenerative-dose protocol. Radiation Measurements 32, 57–73.

Nabel, P.E., Morrás, H.J.M., Petersen, N., Zech, W., 1999. Correlation of magnetic and lithologic features of soils and Quaternary sediments from the undulating Pampa, Argentina. Journal of South American Earth Sciences 12, 311–323.

Naranjo, J.A., Haller, M.J., Ostera, H.A., Pesce, A.H., Sruoga, P., 1999. Geología y peligros del complejo volcánico Planchón-Peteroa, Andes del sur (35, 15 S), región del Maule, Chile—provincia de Mendoza, Argentina, Boletín, vol. 52. Servicio Nacional de Geología y Minería, Santiago.

Polanski, J., 1963. Estratigrafía, neotectónica y geomorfología del Pleistoceno pedemontano entre los ríos Diamante y Mendoza. Revista de la Asociación Geológica Argentina XVII 3–4, 127–349.

Prescott, J.R., Hutton, J.T., 1994. Cosmic ray contributions to dose rates for luminescence and ESR dating: large depths and long-term time variations. Radiation Measurements 23, 497–500.

Prieto, A.R., 1996. Late Quaternary vegetational and climatic changes in the Pampa grassland of Argentina. Quaternary Research 45, 73–88.

Prieto, A.R., 2000. Vegetational history of the Lateglacial-Holocene transition in the grassland of eastern Argentina. Palaeogeography, Palaeoclimatology, Palaeoecology 157, 167–188.

Prohaska, F., 1976. The climate of Argentina, Paraguay and Uruguay. In: Schwerdtfeger, W. (Ed.), World Survey of Climatology 12. Climates of Central and South America. Elsevier, Amsterdam, pp. 13–112.

Quatrocchio, M., Borromei, A., 1998. Paleovegetational and paleoclimatic changes during the Late Quaternary in southwestern Buenos Aires province and southern Tierra del Fuego (Argentina). Palynology 22, 67–82.

Ramos, V., Almeida, A., 2000. Tectonic evolution of the Andes. In: Cordani, U.G., Milani, E.J., Thomaz Filho, A., Campos, D.A. (Eds.), Tectonic Evolution of South America, pp. 635–685.

Ramos, V., Nullo, F.C., 1993. El volcanismo de arco cenozoico. In: Ramos, V.A. (Ed.), XII Congreso Geológico Argentino y II Congreso de Exploración de Hidrocarburos (Mendoza, 1993). Geología y Recursos Naturales de Mendoza, relatorio, vol. 1 (12), pp. 149–160.

Rieck, H.J., Sarna-Wojcicki, A.M., Mayer, C.E., Adam, D.P., 1992. Magnetostratigraphy and tephrochronology of an Upper Pliocene to Holocene record in lake sediments at Tule Lake, Northern California. Geological Society of America Bulletin 104, 409–428.

Sarna-Wojcicki, A.M., Davis, J.O., 1991. Quaternary tephrochronology. In: Morrison, R.B. (Ed.), The Geology of North America: Quaternary Nonglacial Geology; Conterminous United States, Vol. k-2. Geological Society of America, Denver, CO, pp. 93–115.

Smith, J., Vance, D., Kemp, R.A., Archer, C., Toms, P., King, M., Zárate, M., 2003. Isotopic constraints on the source of Argentinian loess—with implications for atmospheric circulation and the provenance of Antarctic dust during recent glacial maxima. Earth and Planetary Science Letters 212, 181–196.

Stern, C., 1990. Tephrochronology of southernmost Patagonia. National Geographic Research 6, 110–126.

Stern, C., 1992. Tefrocronología de Magallanes: nuevos datos e implicaciones. Anales Instituto de la Patagonia 21, 129–141.

Stern, C., Amini, H., Charrier, R., Godoy, E., Herve, F., Varela, J., 1984. Petrochemistry and age of rhyolitic pyroclastic flows which occur along the drainage valleys of the Río Maipo and Río Cahapoal (Chile) and the Río Yaucha and Río Papagayos (Argentina). Revista Geológica de Chile 23, 39–52.

Stokes, S., Lowe, D.J., 1988. Discriminant Function analysis of Late Quaternary tephras from five volcanoes in New Zealand using glass shard major element chemistry. Quaternary Research 30, 270–283.

Teruggi, M.E., 1957. The nature and origin of Argentine loess. Journal of Sedimentary Petrology 217, 322–332.

Teruggi, M.E., Imbellone, P.A., 1987. Paleosuelos loéssicos superpuestos en el Pleistoceno Superior–Holoceno de la región de la Plata, Provincía de Buenos Aires, Argentina. Ciencia del Suelo 5, 176–188.

Turney, C.S.M., Lowe, J.J., Wastegård, S., Cooper, R., Roberts, S.J., 2001. The development of a tephrochronological framework in the last glacial—Holocene transition in NW Europe. In: Juvignè, E., Raynal, J.-P. (Eds.), Tephras: Chronology, Archaeology, Dossiers de l'Archéo-Logis no. 1, Haute-Loire, pp. 101–109.

Wintle, A.G., 1973. Anomalous fading of thermoluminescence in mineral samples. Nature 245, 143–144.

Zárate, M.A., 2000. The Pleistocene/Holocene transition in the eastern Andean piedmont of Mendoza, Argentina. Current Research in the Pleistocene 17, 149–151.

Zárate, M., 2002. Geología y estratigrafía del Pleistoceno tardío-Holoceno

en el piedemonte de Tupungato-Tunuyán, Mendoza, Argentina. XV Congreso Geológico Argentino, 24–26 de abril de 2002, Calafate, Santa Cruz. ACTAS, Argentina, pp. 615–620.

Zárate, M., Blasi, A., 1991. Late Pleistocene–Holocene eolian deposits of the southern Buenos Aires province, Argentina. GeoJournal 24, 211–220.

Zárate, M.A., Kemp, R.A., Blasi, A.M., 2002. Identification and differentiation of Pleistocene paleosols in the northern pampas of Buenos Aires, Argentina. Journal of South American Earth Sciences 15, 303–313.

Zimmerman, D.W., 1971. Thermoluminescent dating using fine grains from pottery. Archaeometry 13, 29–52.